Supplementary information for

Vibrational spectroscopy as a powerful tool to follow-up immunoadsorption therapy treatment of dilated cardiomyopathy - a case report

Jing Huang, †[a,b,c] Anuradha Ramoji, †[a,b,c] Shuxia Guo, [a,b] Thomas Bocklitz, [a,b] Valérie Boivin-Jahns, [d] Jan Möller, [d,e] Michael Kiehntopf, [f] Michel Noutsias, [g,h] Jürgen Popp [a,b,c,i] and Ute Neugebauer *[a,b,c,i]

a. Institute of Physical Chemistry and Abbe Center of Photonics, Helmholtzweg 4, Friedrich-Schiller University, D-07743, Jena, Germany.
b. Leibniz Institute of Photonic Technology, Albert-Einstein-Straße 9, D-07745, Jena, Germany.
c. Center for Sepsis Control and Care, Jena University Hospital, Am Klinikum 1, D-07747, Jena, Germany.
d. Institute of Pharmacology and Toxicology, University of Würzburg, Versbacher Str. 9, 97078 Würzburg, Germany
e Max-Delbrück-Centrum für Molekulare Medizin, Robert-Rössle-Str. 10, 13125 Berlin, Germany
f. Institute of Clinical Chemistry and Laboratory Diagnostics, Jena University Hospital, Am Klinikum 1, D-07747, Jena, Germany.
g. Department of Cardiology - Internal Medicine, Jena University Hospital, Am Klinikum 1, D-07747, Jena, Germany
h. Mid-German Heart Center, Department of Internal Medicine III (KIM-III), Division of Cardiology, Angiology and Intensive Medical Care, University Hospital Halle, Martin-Luther-University Halle, Ernst-Grube-Strasse 40, D-06120 Halle (Saale), Germany
i. InfectoGnostics Research Campus Jena, Centre of Applied Research, Philosophenweg 7, D-07743, Jena, Germany

† J. Huang and A. Ramoji have equal contribution to this work.
* Address correspondence: Core Units of Biophotonics, Centre for Sepsis Control and Care (CSCC), Jena University Hospital, Am Klinikum 1, D07747, Jena, Germany. E-mail: Ute.Neugebauer@med.uni-jena.de

Content:

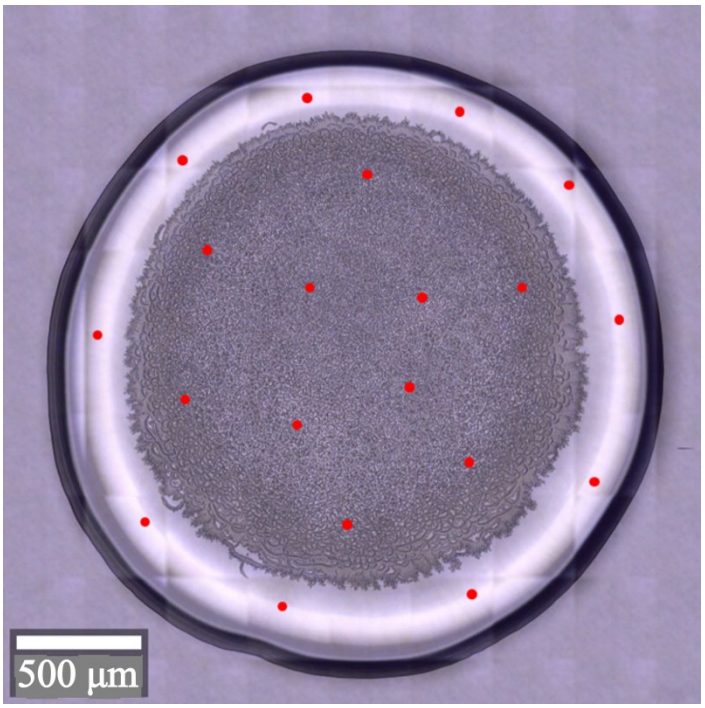

Fig. S1: Mapping scheme of Raman measurement. The red dots indicate positions from where Raman spectra where recorded (sampling spot size ~500 nm).

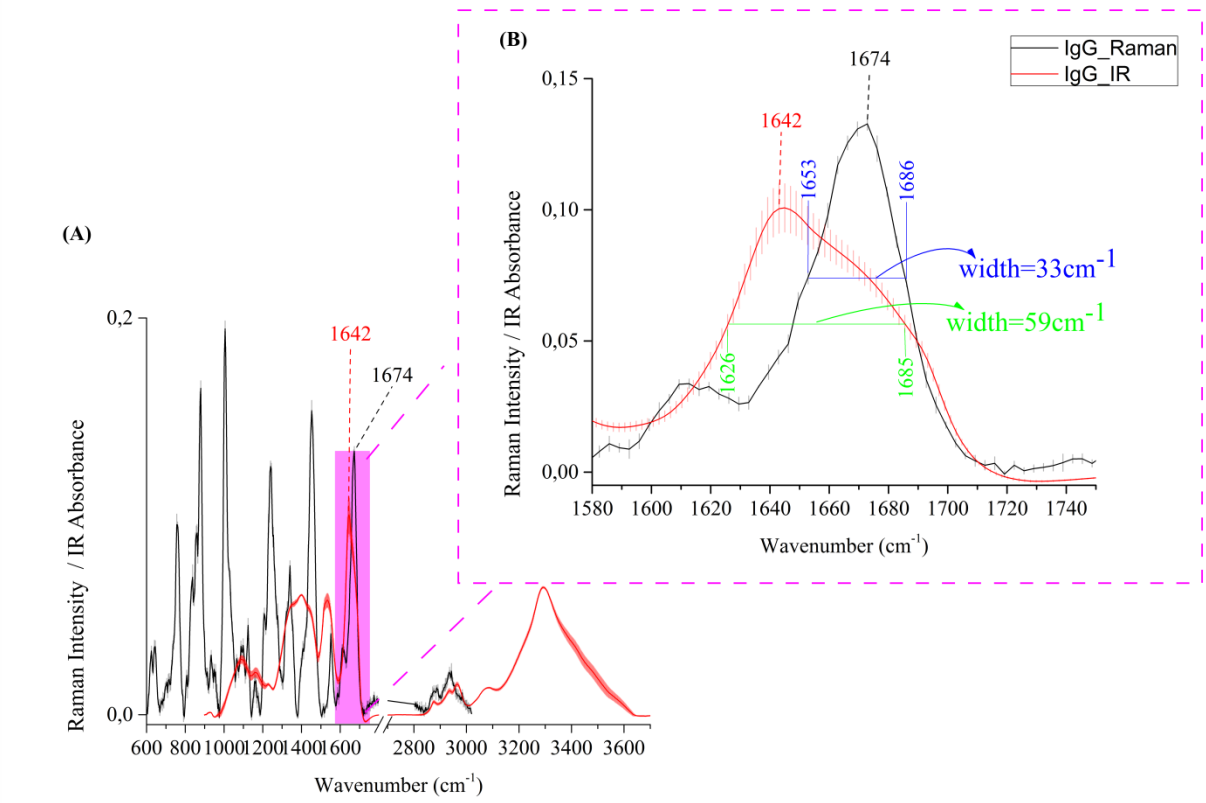

Fig. S2: Bandwidth comparison of amide I in IgG from vibrational spectra: Raman 33cm^{-1}; IR 59cm^{-1}.

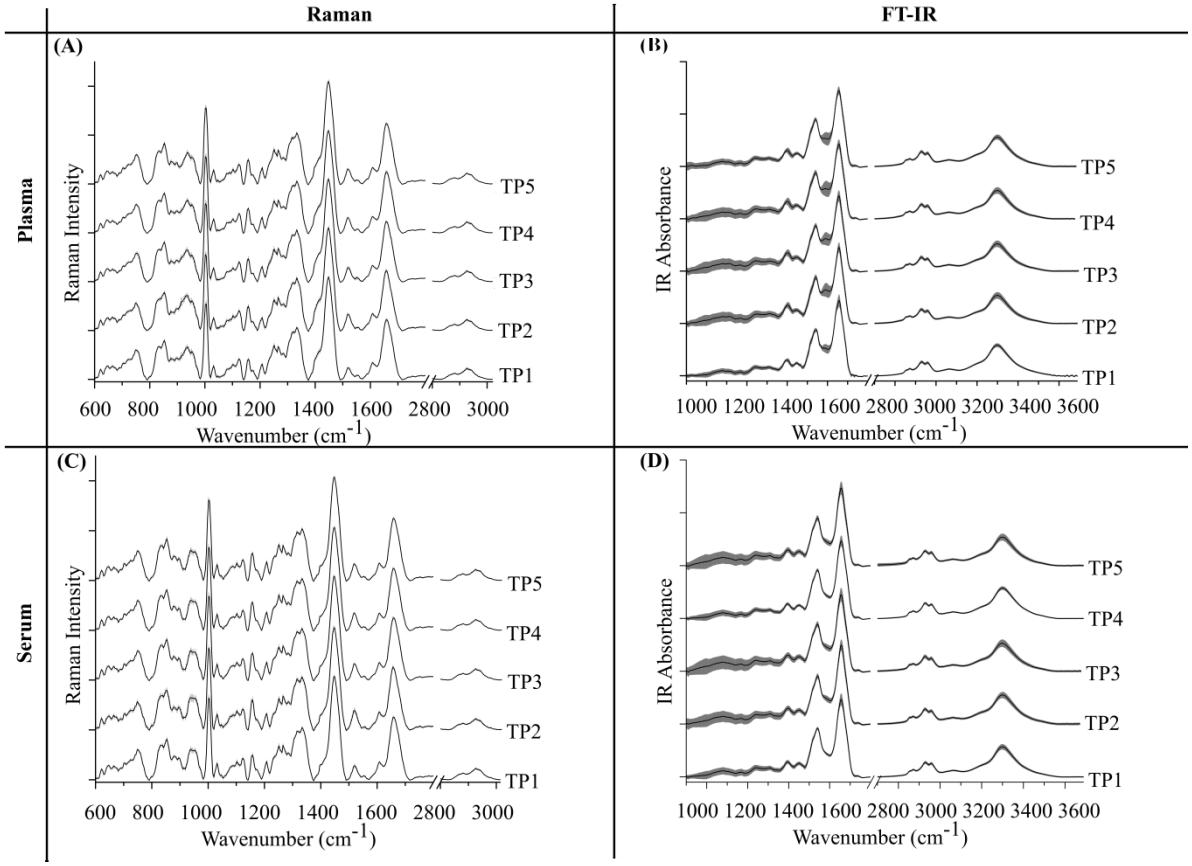

Fig. S3: Mean spectra with standard deviation (shadows) of different time points during IA treatment: left panel: Raman (A, C), right panel: FT-IR (B, D); top panel: plasma (A, B), bottom panel: serum (C, D).

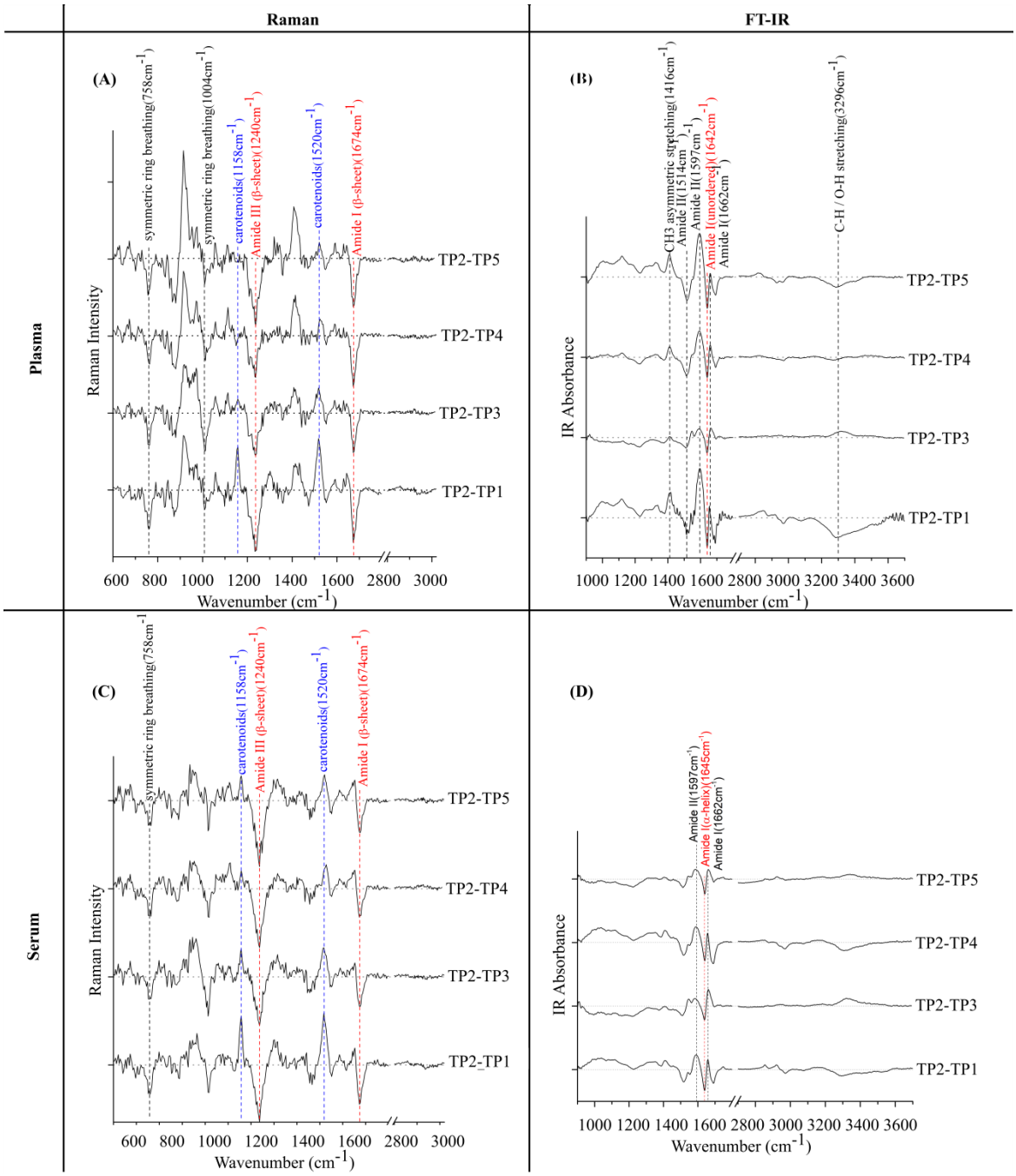

Fig. S4: Difference spectra between TP2 and other time points during IA treatment: left panel: Raman (A, C), right panel: FT-IR (B, D); top panel: plasma (A, B), bottom panel: serum (C, D).

A similar pattern can be seen for all computed difference spectra. For Raman spectra, dominant variations occur around 1158cm^{-1} (positive), 1240cm^{-1} (negative), 1520cm^{-1} (positive) and 1674cm^{-1} (negative). For FT-IR spectra, significant changes show in 1597cm^{-1} (positive), 1642cm^{-1} (negative) and 1662cm^{-1} (positive).The negative bands imply higher spectral intensities in other time points than at TP2, while positive bands mark spectral features that are more prominent in TP2. The positive bands around 1158cm^{-1} and 1520cm^{-1} from Raman spectra might indicate that carotenoids increase immediately after IA therapy (difference spectra TP2-TP1), thereafter decrease (difference spectra TP2-TP3, TP2-TP4, TP2-TP5). Negative bands around 1240cm^{-1} and 1674cm^{-1} from Raman spectra and 1642cm^{-1} from FT-IR spectra should be due to variations of immunoglobulin G during IA treatment. The concentration of anti-cardiac antibodies (and related immunoglobulins) is expected to be lowest at time point 2 due to active removal during therapy, and increase after time point 3 as a result of IgG restoration.

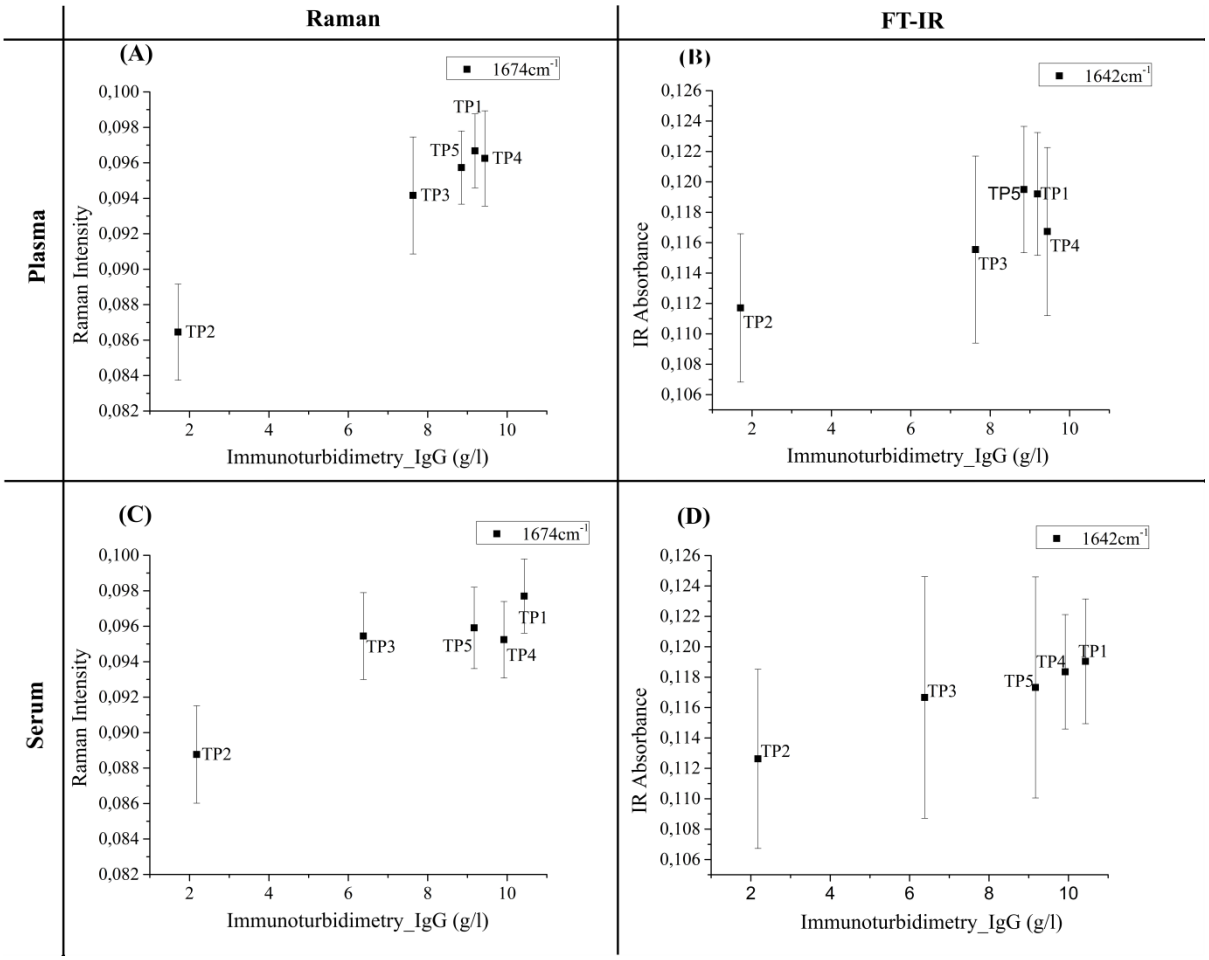

Fig. S5: Correlation of vibrational bands with IgG content. Left panel: Raman (A, C), right panel: FT-IR (B, D); top panel: plasma (A, B), bottom panel: serum (C, D).

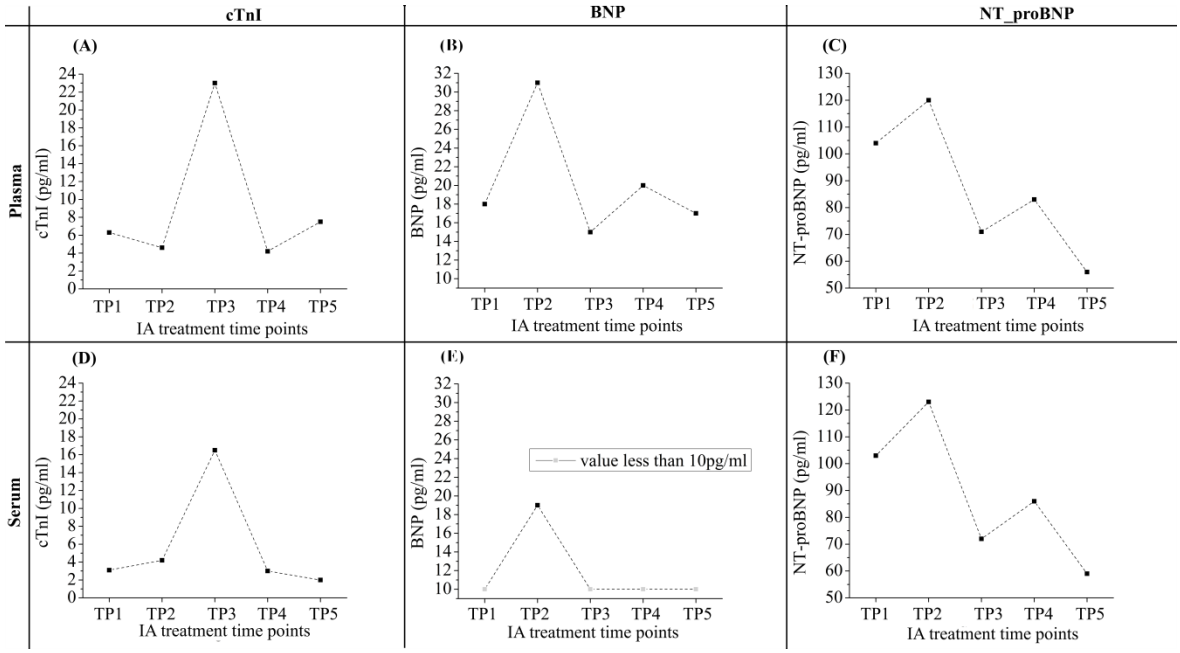

Fig. S6: Variations of cardiac biomarkers responding to different IA time points: left panel: cTnI (A, D), middle panel: BNP (B, E), right panel: NT-proBNP (C, F); top panel: plasma (A, B, C), bottom panel: serum (D, E, F).

Theoretically, the concentration of cardiac biomarkers should be high before IA and decrease after IA responding to the improvement of heart function resulting from the treatment. Three commonly used cardiac biomarkers (cTnI, BNP and NP-proBNP) were measured and the variations are shown in Fig. S6. The changes of cTnI and BNP do not accordance with the theoretical one. This disagreement might have following explanations: (1) Concentrations of these cardiac biomarkers from this DCM patient are under normal ranges. From literatures, cut-off points of cTnI, BNP and NP-proBNP ($\geqslant$ 50 years old) for diagnosing heart failure in females are less than 15.6pg/ml, 100pg/ml and 125pg/ml respectively.[1,2] (2) The decay of plasma and serum samples during the storage at -80°C for long time ($\geqslant$ 2 years) (3) The anti-cardiac antibodies in this patient might not against these three cardiac biomarkers. From literatures, the anticardiac antibodies that have been identified are against G-protein-linked receptors, cardiac myosin, cardiac beta-1 receptors and troponin I. [3-6]

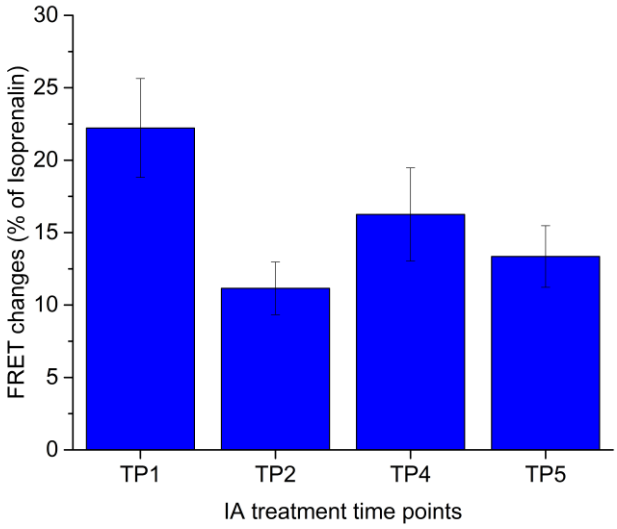

Fig. S7: Anticardiac antibody concentrations as visualized by FRET changes (in% of isoprenalin) for the IgG extracts from blood serum of the DCM patient for the different time points during immunadsorption therapy treatment. Depicted values are averages from four measurements.

To determine the presence and activity of anti-β1-abs *via* receptor-induced cAMP accumulation in β1-AR expressing HEK293 cells, a modified fluorescent cAMP sensor was used (Epac1-camps) [7]. The cells were double stable transfected with both constructs (β1-AR and Epac1) and monoclonal selected based on the largest amplitude upon stimulation. The Epac-sensor detects intracellular cAMP with high spatial and temporal resolution by changes in FRET between CFP and YFP fused to the cAMP binding site of Epac1. The sensor was optimized, using brighter fluorophore-variants with higher quantum yield, to allow a robust and unbiased measurement of samples in 96-well plates. All assays were carried out with IgG-fractions isolated by caprylic acid precipitation, dialysed against PBS and incubated at a 1/10 dilution. At the end of each measurement, the cAMP accumulation achieved by 100 nM (-) isoprenalin was set to the maximal β1-AR response (100% FRET change).

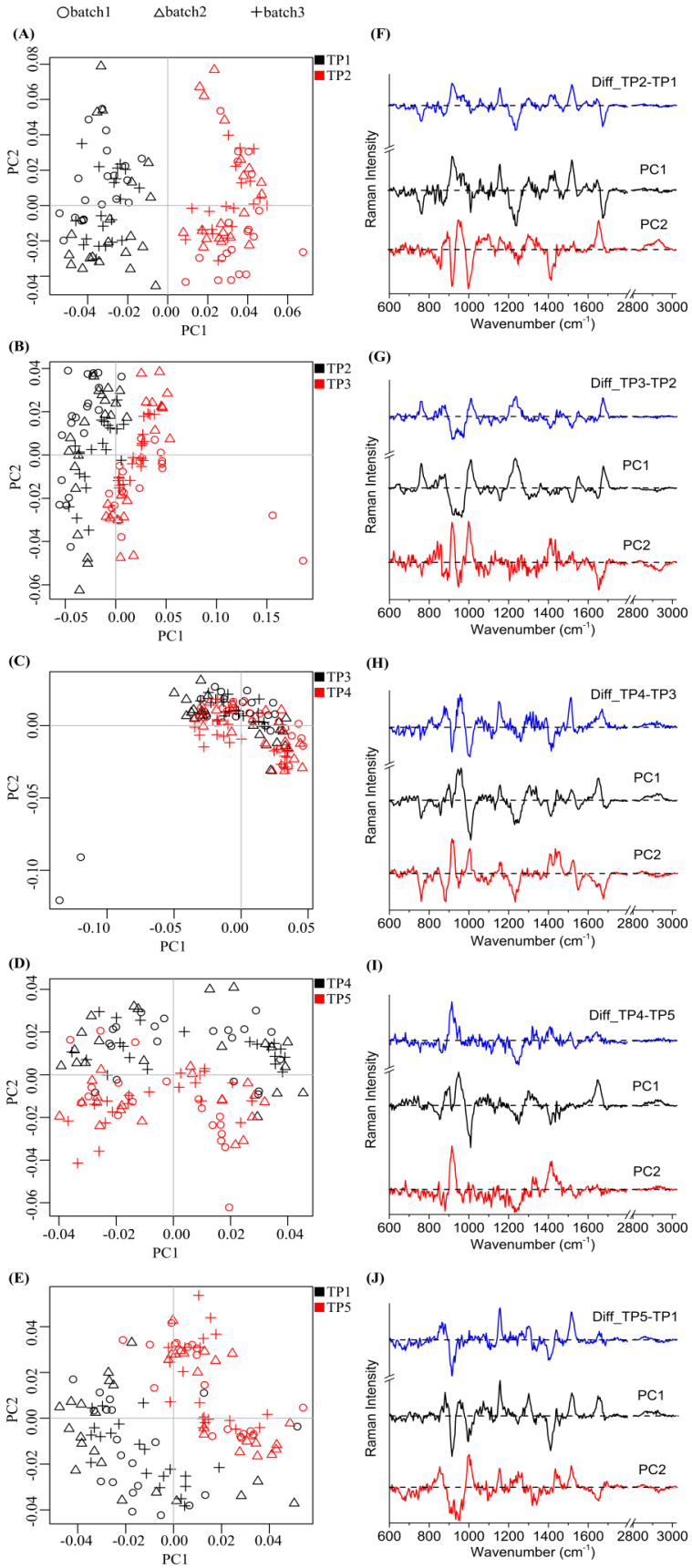

Fig. S8: Pairwise PCA and corresponding difference spectra between sequentially time points for Raman data based on plasma sample: TP1 *vs* TP2 (A, F), TP2 *vs* TP3 (B, G), TP3 *vs* TP4 (C, H), TP4 *vs* TP5 (D, I), TP1 *vs* TP5 (E, J).

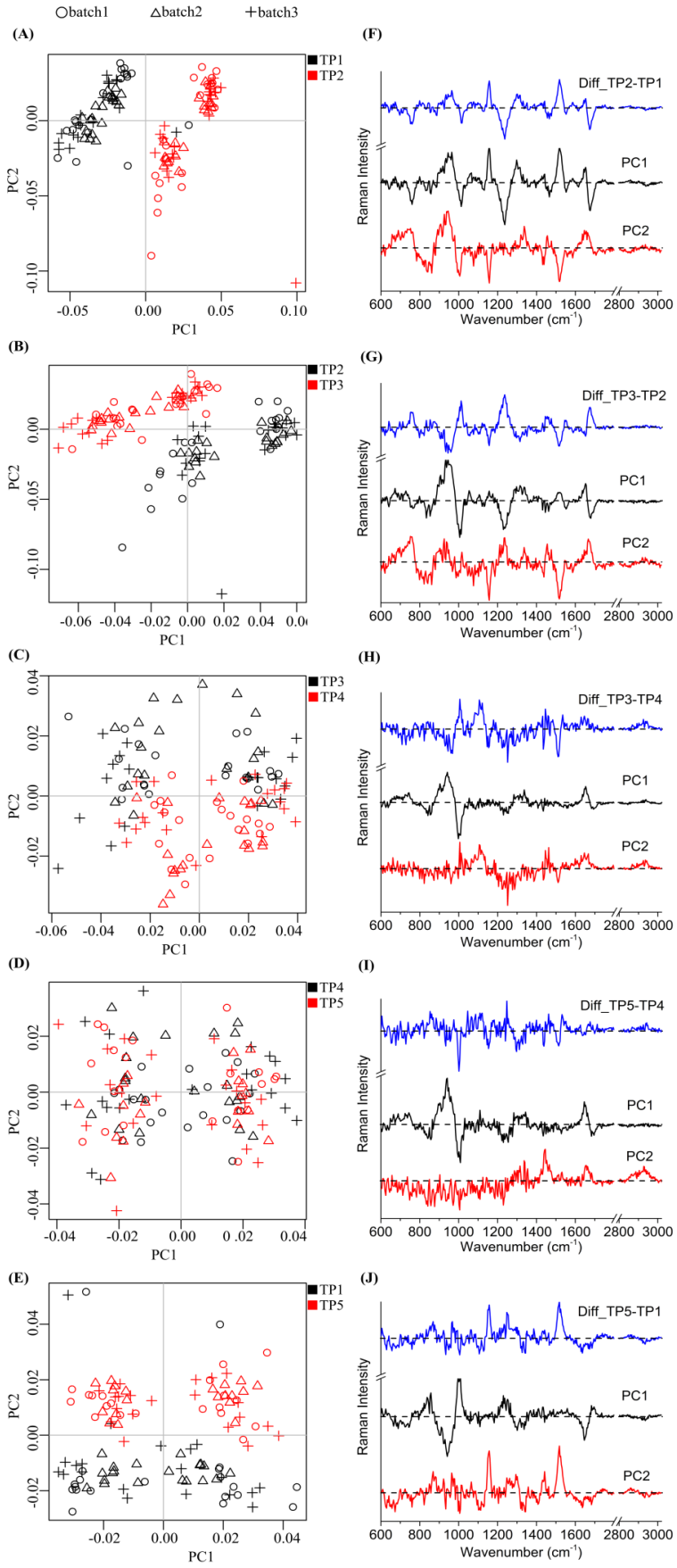

Fig. S9: Pairwise PCA and corresponding difference spectra between sequentially time points for Raman data based on serum sample: TP1 *vs* TP2 (A, F), TP2 *vs* TP3 (B, G), TP3 *vs* TP4 (C, H), TP4 *vs* TP5 (D, I), TP1 *vs* TP5 (E, J).

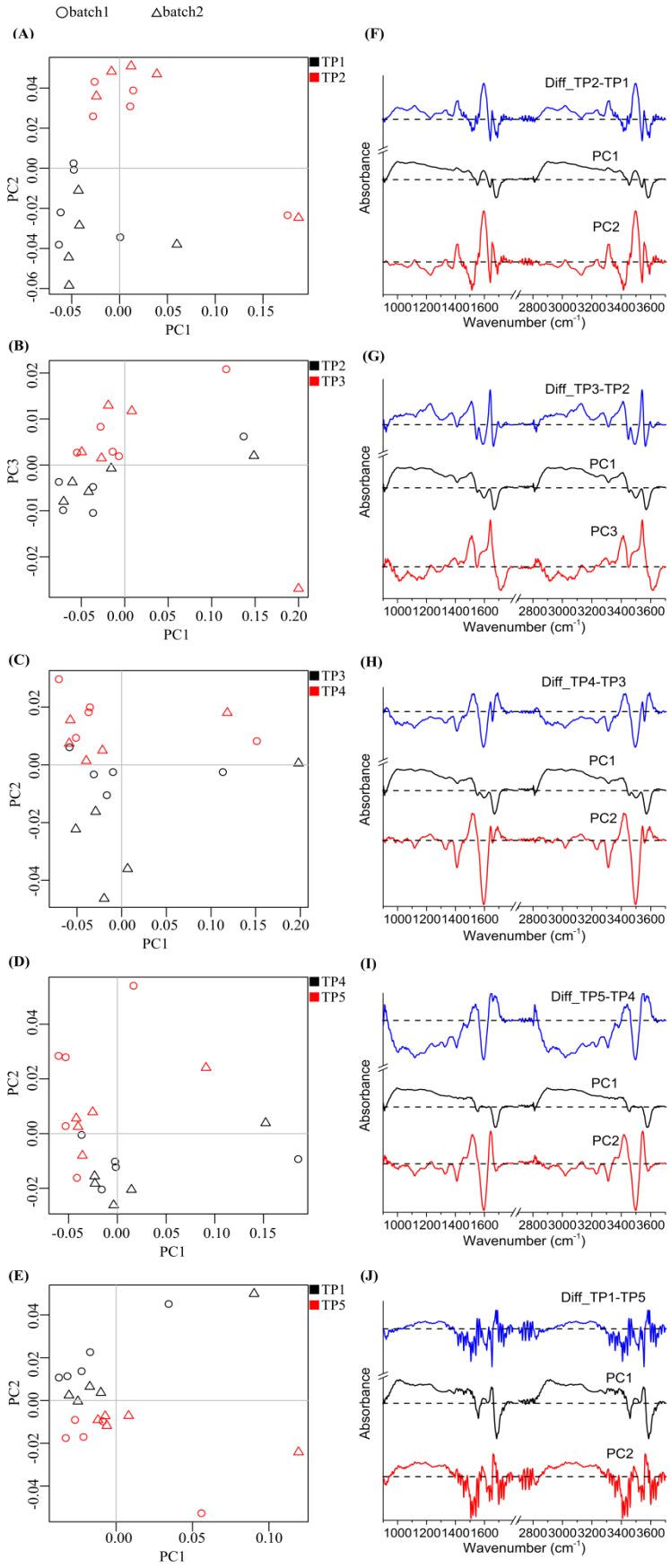

Fig. S10: Pairwise PCA and corresponding difference spectra between sequentially time points for FTIR data based on plasma sample: TP1 vs TP2 (A, F), TP2 vs TP3 (B, G), TP3 vs TP4 (C, H), TP4 vs TP5 (D, I), TP1 vs TP5 (E, J).

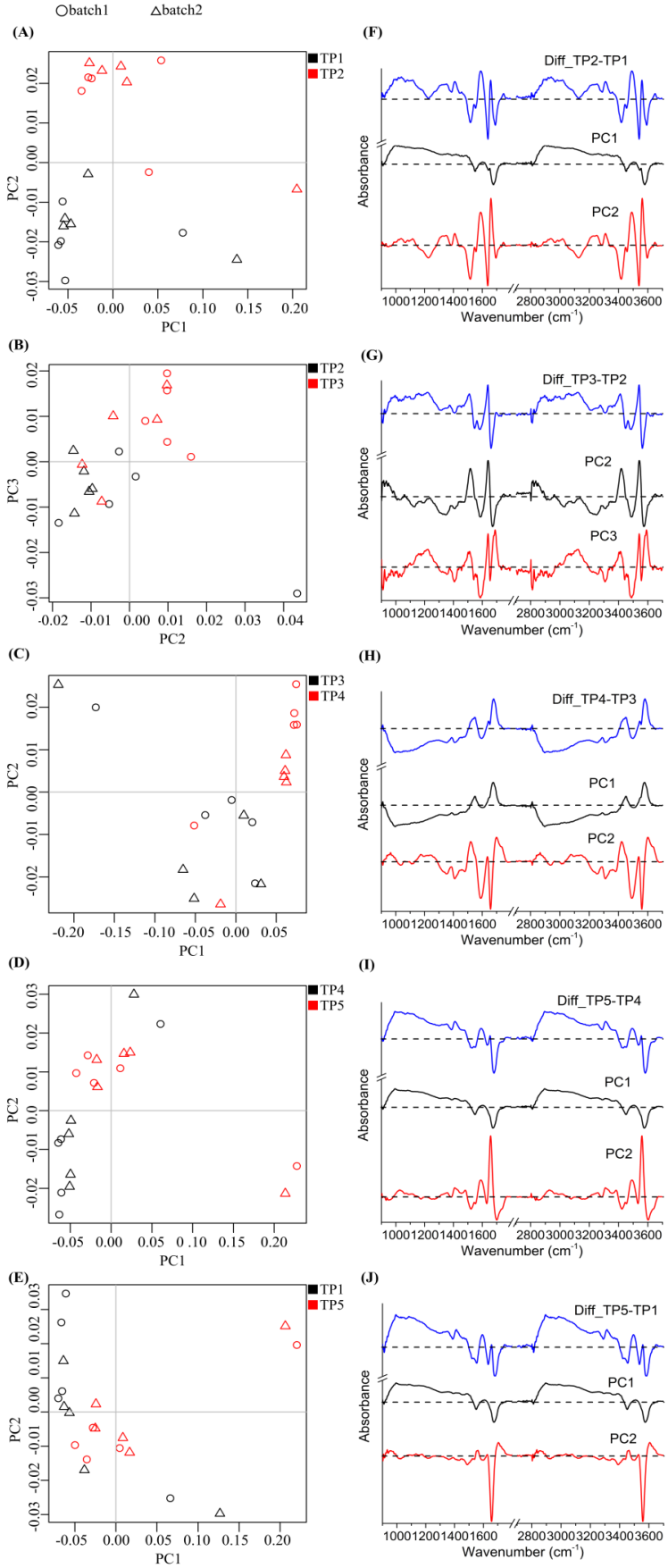

Fig. S11: Pairwise PCA and corresponding difference spectra between sequentially time points for FTIR data based on serum sample: TP1 *vs* TP2 (A, F), TP2 *vs* TP3 (B, G), TP3 *vs* TP4 (C, H), TP4 *vs* TP5 (D, I), TP1 *vs* TP5 (E, J).

Table S1: Tentative assignment of Raman [8-10] and IR bands [11-15] based on literature

Raman band (cm^{-1})	IR band (cm^{-1})	Protein	Nucleic acid	Lipids	Carbohydrate
758		Tryptophan (symmetric ring breathing)			
854		Try, Pro, tyrosine (ring breathing)			
939		C-C stretching backbone (α-helix)			
1004		Phenylalanine (symmetric ring breathing)			
1032		Phe (C-H in plane bending)			
	1038	v C-0	DNA, RNA		Deoxyribose/ribose
	1078	C-O stretching	PO^-_2 symmetric stretching/ DNA, RNA		Glycogen (C-O stretching) /deoxyribose/ribose
	1118		C-O stretching of RNA	Lipids	
1124		C-N stretching		C-C stretching	
1158		Carotenoids (C=C)/C-C/C-N stretching			
	1170			Ester C-O asymmetric stretching	
1209		Phe, Tyr($C-C_6H_5$ stretching)			
1240	1220-1330	Amide III			
1252		Amide III		=CH deformation	
1268		Amide III			
1318		C-H deformation, collagen	G	CH_3CH_2 twist	
1334		CH_3CH_2 wagging	CH_3CH_2 wagging		
	1392	CH_3 deformation		Lipids	
	1398	C=O stretching of COO-			
	1400	Proline/valine			
	1416			CH_3 asymmetric stretching	
1434				CH_2	
1448		CH_2 bending		CH_2 bending	
	1452	CH_2 scissoring			
	1514	Amide II (ß-sheet structures)/δ N-H/ v C-N			
1520		Carotenoids (C=C vibration)			
	1535	CH2 bending/ Amide II		CH_2 bending	
1552	1554	Amide II			
	1589	Amide II			
	1642	Amide I (unordered)			
	1655	Amide I (antiparallel ß-sheet/aggregated strand)			
1659	1662	Amide I			
1674		Amide I (ß-sheet)			
	1695	Amide I (antiparallel b-sheet/aggregated strand)			
	2872	CH_3 symmetric stretching			
	2920	CH_2 symmetric stretching			
	2929			Lipids	
2934		CH_2 symmetric stretching			
	2958	CH_3 asymmetric stretching			
	3282	H-O-H stretching			
	3296	C-H stretching/O-H stretching			

Table S2: Identification of SVM classification model on single spectra level with combined treatment groups

True \ Prediction		Raman					IR			
		Before IA	After IA	Follow-up of IA	**Sensitivity**		Before IA	After IA	Follow-up of IA	**Sensitivity**
		TP1	TP2	TP3-TP5			TP1	TP2	TP3-TP5	
Plasma	TP1	**20**	0	0	**100.00%**		**4992**	0	8	**99.84%**
	TP2	0	**19**	1	**95.00%**		0	**4927**	73	**98.54%**
	TP3-TP5	1	0	**59**	**98.33%**		45	121	**14834**	**98.89%**
	Specificity	**98.75%**	**100.00%**	**97.50%**			**99.78%**	**99.40%**	**99.19%**	
	Accuracy	**98.00%**					**99.01%**			
Serum	TP1	**18**	0	2	**90.00%**		**4930**	18	52	**98.60%**
	TP2	0	**17**	3	**85.00%**		0	**4994**	6	**99.88%**
	TP3-TP5	2	0	**58**	**96.67%**		274	235	**14491**	**96.61%**
	Specificity	**97.50%**	**100.00%**	**87.50%**			**98.63%**	**98.74%**	**99.42%**	
	Accuracy	**93.00%**					**97.66%**			

References

1. E. Braunwald, N Engl J Med, 2008, 358, 2148-59.
2. W. C. Chen, K. D. Tran and A. S. Maisel, Heart, 2010, 96, 314-20.
3. M. Noutsias and B. Maisch, Myocarditis and pericarditis. In: M. Tubaro, P. Vranckx, S. Price and C. Vrints, editors. The ESC Textbook of Intensive and Acute Cardiacvascular care. 2nd Ed. Oxford: Oxford university press; 2015. p. 547-60.
4. S. B. Felix, A. Staudt, Int J Cardiol, 2006, 112, 30-3.
5. A. Staudt, Y. Staudt, M. Dörr, M. Böhm, F. Knebel, A. Hummel, L. Wunderle, M. Tiburcy, K. D. Wernecke, G. Baumann and S. B. Felix, J Am Coll Cardiol, 2004, 44, 829-36.
6. S. B. Felix, A. Staudt, M. Landsberger, Y. Grosse, V. Stangl, T. Spielhagen, G. Wallukat, K. D. Wernecke, G. Baumann and K. Stangl, J Am Coll Cardiol, 2002, 39, 646-52.
7. V. O. Nikolaev, M. Bünemann, L. Hein, A. Hannawacker and M. J. Lohse. J Biol Chem., 2004, 279(36), 37215-8.
8. K. W. Poon, F. M. Lyng, P. Knief, O. Howe, A. D. Meade, J. F. Curtin, H. J. Byrne and J. Vaughan, Analyst, 2012, **137**, 1807-14.
9. U. Neugebauer, S. Trenkmann, T. Bocklitz, D. Schmerler, M. Kiehntopf and J. Popp, J Biophoton, 2014, **7**, 232-40.
10. A. Weselucha-Birczynska, M. Kozicki, J. Czepiel and M. Birczynska, Analyst, 2013, **138**, 7157-63.
11. J. R. Hands, K. M. Dorling, P. Abel, K. M. Ashton, A. Brodbelt, C. Davis, T. Dawson, M. D. Jenkinson, R. W. Lea, C. Walker and M. J. Baker, J Biophoton, 2014, **7**, 189-99.
12. F. Bonnier, M. J. Baker and H. J. Byrne, Anal Methods, 2014, **6**, 5155-60.
13. W. Petrich, K. B. Lewandrowski, J. B. Muhlestein, M. E. Hammond, J. L. Januzzi, E. L. Lewandrowski, R. R. Pearson, B. Dolenko, J. Früh, M. Haass, M. M. Hirschl, W. Köhler, R. Mischler, J. Möcks, J. Ordonez-Llanos, O. Quarder, R. Somorjai, A. Staib, C. Sylven, G. Werner and R. Zerback, Analyst, 2009, **134**, 1092-8.
14. G. L. Owens, K. Gajjar, J. Trevisan, S. W. Fogarty, S. E. Taylor, B. Da Gama-Rose, P. L. Martin-Hirsch and F. L. Martin, J Biophoton, 2014, **7**, 200-9.
15. K. Thumanu, S. Sangrajrang, T. Khuhaprema, A. Kalalak, W. Tanthanuch, S. Pongpiachan and P. Heraud, J Biophoton, 2014, **7**, 222-31.